

# Effect of sulfate-ester content and nanocellulose allomorph on stability of amylopectin-xyloglucan water-in-water emulsions

Cassiano Pires, Bernardo Mauad Régnier, Maria Jackeline Rodrigues dos Santos, Rilton Alves de Freitas\*

BioPol, Pharmacy Department, Federal University of Paraná, 80210-170, Curitiba, Paraná, Brazil

## ARTICLE INFO

### Keywords:

Water-in-water emulsions  
Nanocellulose  
Polysaccharides  
Pickering stabilization

## ABSTRACT

The effect of sulfate ester content on type I allomorph cellulose nanoparticles (CNPs) surface was evaluated in water-in-water emulsions with amylopectin (AMP) dispersed in xyloglucan (XG) phase. In addition, effect of cellulose allomorph type II was also verified. From a single source: microcrystalline cellulose (MCC) sulfated CNPs were isolated by sulfuric acid hydrolysis and subsequently sulfate content was modulated on CNPs surface with partial and quasi-total desulfation, keeping a rod-like particle morphology. MCC was solubilized with phosphoric acid and precipitated in water generating type II spherical nanocellulose allomorph. Particles were characterized by AFM, XRD, zeta potential and their surface groups were quantified by conductometric titration. Effect of adding these particles was evaluated at different concentrations in the phase diagram where XG is continuous phase. It was revealed that sulfated CNPs preference interact with XG increasing its viscosity and stabilizing the emulsions regardless their superficial sulfate content. On the other hand, phosphated nanocellulose interacts less with XG allowing it to migrate to XG-AMP interface and partially stabilize emulsions by Pickering effect.

## 1. Introduction

Water-in-water (w/w) emulsions can be understood as interesting colloidal systems in which two hydrophilic polymers are dispersed in water and phase separate segregated (Beldengrün et al., 2020; Esquena, 2016). This phenomenon of segregation is very common for macromolecules mixtures such as biopolymers and is frequently found in many food systems (Frith, 2010; Norton & Frith, 2001).

An inherent characteristic of these mixtures is that their interface presents lengths scales greater than length of surfactants molecules which makes their use unfeasible for w/w emulsion stabilization (Nicolai & Murray, 2017). Therefore, as an alternative, particles can be adsorbed at liquid-liquid interface forming Pickering emulsions, and promoting an emulsion metastable state. There is a large variety of particles for emulsion stabilization and several parameters can be evaluated such as morphology, size, pH, particle-polymer interactions (Balakrishnan, Nicolai, Benyahia, & Durand, 2012; Gonzalez-Jordan, Nicolai, & Benyahia, 2016; Nguyen, Wang, Saunders, Benyahia, & Nicolai, 2015; Vis et al., 2015).

Mixtures of amylopectin (AMP) and xyloglucan (XG) produced a

very interesting example of w/w emulsion. de Freitas, Nicolai, Chassenieux, and Benyahia (2016) used  $\beta$ -lactoglobulin microgels ( $\beta$ LGm) and achieved system stability at  $\text{pH} \leq 5.0$ , exactly at particle isoelectric point (IP). For higher values of pH AMP is the preferred phase for  $\beta$ LGm, and particles cannot migrate to interface. Another way to modify the  $\beta$ LGm preference for AMP phase distribution was proposed by Hazt et al. (2020) through particle morphology modification. Results showed full stabilization at pH 6 and partial at pH 7 for fibrils instead spherical ones, limited to  $\text{pH} \leq 5.0$ . Both studies demonstrated that stabilization can be improved by changing particles properties and their interaction with both phases.

Here, our hypothesis is that cellulose particles could bring stability to AMP/XG emulsions, acting as an interesting and alternative source of particles with variable properties, and able to produce a green emulsion. Cellulose is the most abundant biopolymer in the world found in a wide variety of sources such as plants, animals and bacterias. Due to the large hydroxyls in its structure formed by monomers that consist of 1,4- $\beta$ -D-glucose units, numerous hydrogen bonds can be formed and van der Waals interactions create regions of high chain ordering (crystalline) or disordered (amorphous) regions (Habibi, Lucia, & Rojas, 2010).

\* Corresponding author.

E-mail address: [rilton@ufpr.br](mailto:rilton@ufpr.br) (R. Alves de Freitas).

Cellulose can be isolated into nanoparticles known as nanocelluloses or cellulose nanoparticles (CNPs) (Dufresne, 2013; Foster et al., 2018; Habibi et al., 2010) and these materials can change their morphology, size, surface chemistry, and other characteristics depending on their origin, treatment and post-treatment providing a wide range of possible applications as Pickering particles (Trache et al., 2020).

Nanocellulose was used previously as Pickering particles for w/w emulsions stabilization, for example bacterial cellulose nanofibers (Lei et al., 2022) and rod-like cellulose nanocrystals (Ben Ayed et al., 2018; Peddireddy, Nicolai, Benyahia, & Capron, 2016; Zhou et al., 2023), demonstrating ability to act as Pickering particles.

However, the cellulose nanoparticles were never evaluated in AMP/XG emulsions, and an important feature is that XG could interact with cellulose nanoparticles modulated by the sulfate content according to Pirich et al. (2015). The authors noted that cellulose nanoparticles isolated with 0.65 wt% sulfate content interact with XG forming unstable layers, favoring desorption. By another way, cellulose nanocrystals with lower sulfate contents shows a favorable interaction and exhibits a good colloidal stability compared to cellulose nanocrystals without sulfate content.

Supported by the fact that the interactions between XG and cellulose nanocrystals are modulated by sulfate content of particles our main hypothesis in this work is that by modulating the sulfate content on cellulose nanoparticles through isolation with sulfuric acid and subsequent sulfate stripping (desulfation) we can modulate the interactions between XG and CNPs. In this manuscript, the acronym CNPs was selected since some particles produced are not crystals, and to avoid mistakes the term CNPs was used throughout the manuscript.

Based on this hypothesis, the main questions we expected to answer are:

- 1) Is it possible to distribute CNPs to liquid-liquid interface forming Pickering emulsions, avoiding coalescence and phase separation, modulating sulfate content?
- 2) Could the cellulose allomorph affect the particle-polysaccharide phases interactions?

To test our hypothesis, CNPs were isolated from commercial microcrystalline cellulose (MCC) using sulfuric acid hydrolysis and through subsequent desulfation. After that, different particles concentrations with different sulfate contents were tested on AMP-XG emulsions. Sulfate content and also the nanocellulose nanoparticle structure will be discussed in this paper. Also, MCC were solubilized with phosphoric acid and, after regeneration, CNPs with other morphologies and crystalline structures were produced, and these particles were also tested in w/w emulsions.

## 2. Materials and methods

### 2.1. Cellulose nanoparticles isolation

Sulfated and phosphated cellulose nanoparticles (CNPs) were isolated from a single commercial MCC source (Blanver, São Paulo, Brazil), using two distinct conditions: hydrolysis with sulfuric or phosphoric acid. Two suspensions were isolated: CNP-SH (sulfuric acid hydrolysis) and CNP-PH (phosphoric acid hydrolysis). Part of the CNP-SH suspension was subjected to partial desulfation with hydrochloric acid (CNP-D2) and complete desulfation through solvolysis (CNP-S1).

#### 2.1.1. Cellulose nanoparticles isolation: sulfuric acid hydrolysis

Reaction conditions for this hydrolysis were adapted from the procedure described by Bondeson, Mathew, and Oksman (2006). First, 100 mL of 64 wt % sulfuric acid solution was heated at 45 °C, using oil bath. Then, 10 g of MCC powder was carefully added under mechanical stirring, using a PTFE anchor stirrer, under 3000 rpm, and the reaction took place over 2 h. To stop the hydrolysis, the flask was submerged in an ice

bath and 1 L of cooled water (4 °C) was added. The suspension was centrifuged for 10 min at  $1,1 \times 10^4$  g, at 20 °C. Supernatant was discarded, and the precipitate resuspended with purified water. This process was repeated three times. Then, suspension was dialyzed against purified water using dialysis membranes (Sigma-Aldrich, cutoff 14 kg mol<sup>-1</sup>) to remove the excess of acid. This step took three days until the pH suspension was constant. Final concentration of CNP-SH suspension was determined by gravimetric analysis, and it was kept in suspension and stored in a refrigerator at 4 °C.

#### 2.1.2. Cellulose nanoparticles desulfation

**2.1.2.1. Partial desulfation.** Conditions for partial desulfation were adapted from Jiang, Esker, and Roman (2010). A 225 µL of hydrochloric acid solution (11.7 mol L<sup>-1</sup>) was added to 70 mL of 1.5 wt % CNP-SH suspension. Reaction took place for 2.5 h at 80 °C, under mechanical stirring. Then, suspension was subjected to dialysis as described in section 2.1. This procedure was repeated once more, resulting in a suspension of nanoparticles (CNP-D2) that underwent two cycles of desulfation.

**2.1.2.2. Quasi-total desulfation.** Initially, 70 mL of the 1.5 wt % CNP-SH suspension was neutralized with 60 µL of pyridine and subsequently lyophilized. Resulted material was suspended in 90 mL of dimethyl sulfoxide and sonicated for 10 min at 20% amplitude in an ice bath. After dispersion, 10 mL of methanol was added, and suspension was stirred under mechanical agitation for 2 h at 80 °C. After that 100 mL of cold purified water (4 °C) was added to the reaction and the suspension was subjected to dialysis as described in section 2.1 resulting in a CNC-S1 sample.

#### 2.1.3. Cellulose nanoparticles isolation: phosphoric acid hydrolysis

For hydrolysis with phosphoric acid, the reaction conditions were adapted from Hao et al. (2015). Therefore, 200 mL of 85 wt % phosphoric acid solution was heated to 58 °C in oil bath. Next, 5 g of MCC were added and the mixture was stirred with a PTFE anchor on a mechanical stirrer, at 3.000 rpm. After 1 h the mixture was added to 1 L of purified water at 4 °C. The CNP-PH suspension was centrifuged and dialyzed under the same conditions as the hydrolysis with sulfuric acid (section 2.1.1) and it was kept in suspension and stored in a refrigerator at 4 °C.

#### 2.1.4. Cellulose nanoparticles characterization

**2.1.4.1. Conductometric titration.** Conductometric titration was performed for sulfate or phosphate quantification in cellulose nanoparticles. For this, concentration of suspensions was set to 0.5 wt % and were sonicated for 60 s at 20% amplitude in an ice bath. Prior to titration, all suspensions were eluted on a cation exchange resin column as reported by Beck, Méthot, and Bouchard (2015). Samples were titrated against a 2.01 mmol L<sup>-1</sup> standardized NaOH solution and conductivity was read in a conductivity meter (Alfakit AT-255, Capoeiras, Brazil). For each suspension of cellulose nanoparticles, three independent measurements (runs) were performed. The value of the sulfate or phosphate content is obtained from (Eq. (1)).

$$\sigma = \frac{V_{NaOH} C_{NaOH}}{m_{susp} C_{susp}} \quad (1)$$

Were  $\sigma$  the value of sulfate or phosphate, in mol kg<sup>-1</sup>,  $V_{NaOH}$  and  $C_{NaOH}$  are the volume and concentration of sodium hydroxide and  $m_{susp}$  and  $C_{susp}$  are the mass and concentration (mass %) of suspensions, respectively.

**2.1.4.2. Atomic force microscopy.** Topography images were obtained with Agilent Scanning Probe Microscopy 5500 equipment (Keysight,

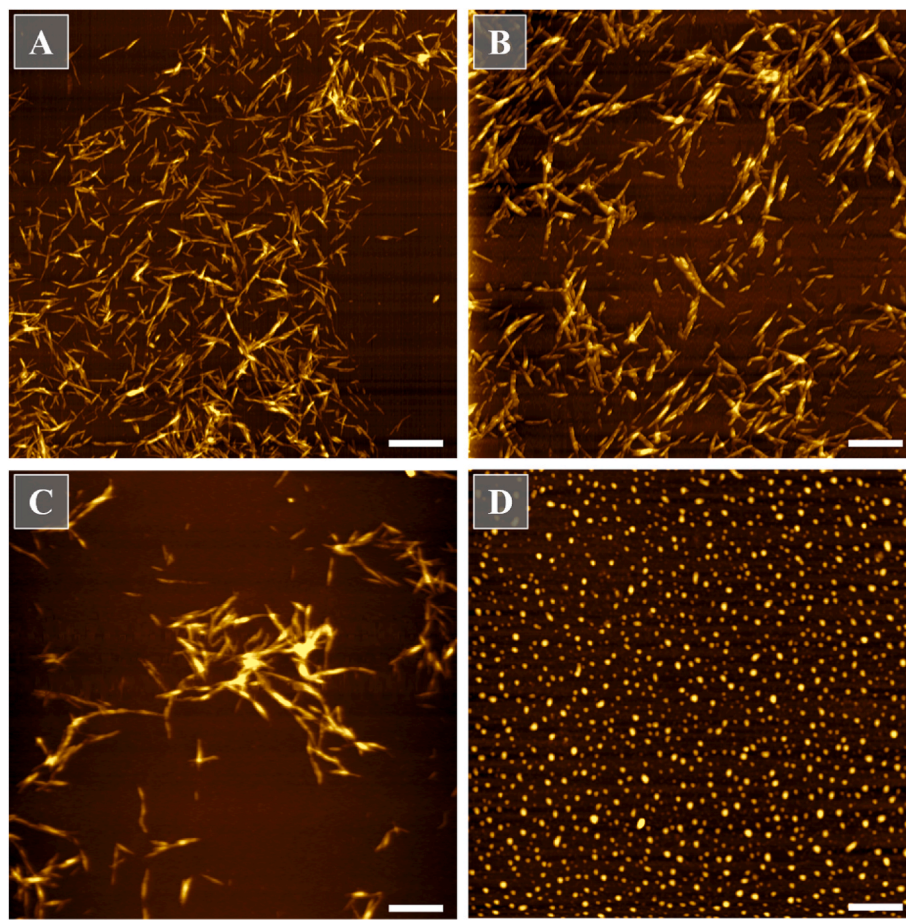


**Fig. 1.** Topography images obtained by atomic force microscopy for nanocelluloses isolated from microcrystalline cellulose: (A) CNP-SH hydrolyzed with sulfuric acid; (B) CNP-D2, partially desulfated; (C) CNP-S1 quasi-totally desulfated and (D) CNP-PH solubilized in phosphoric acid and precipitated in water. The scale bar represents 500 nm.

Santa Rosa, USA) operating in intermittent contact method, with NSC35–AlBS cantilever (Mikromasch, Watsonville, USA), with  $8.9 \text{ N m}^{-1}$  force constant and 200 kHz resonance frequency. A volume of 100  $\mu\text{L}$  of diluted suspension (0.02 wt %) was deposited on freshly mica substrate ( $2 \times 2 \text{ cm}$ ) and left to stand for 60 s at room temperature. Then, they were subjected to spin coating (1600 rpm, 20 s). This procedure was repeated once more. Samples were left to dry overnight at room temperature. Images were obtained using the PicoView 14.4 software and later analyzed using the Gwyddion 2.52 software.

**2.1.4.3. Dynamic light scattering.** Aggregation and disaggregation experiments for CNP-PH sample were evaluated using the NanoDynamic DLS flow mode technique performed at a Brookhaven Nano Particle Size Analyzer, (BI-Nano DLS, New York, USA) operating at  $90^\circ$  scattered light detector with a 35 mW solid state 632.8 nm laser wavelength. The 0.1 wt % CNP-PH suspension was sonicated (Sonics Vibra Cell, Connecticut, USA) for 120 s at 25% amplitude (800 J) before analysis or sonicates, at same conditions, for full time measurement. In the last case, samples were pumped from the sonicator cell by peristaltic pump at a flow rate of  $100 \mu\text{L min}^{-1}$ . Hydrodynamic radius measurement was observed over the duration of 5 min.

**2.1.4.4. X-Ray diffraction (XRD).** Diffraction patterns of MCC and cellulose nanoparticles were analyzed by X-Ray diffraction with Shimadzu (XRD 6000, Japan) operating at 40 kV voltage and 20 mA current with Cu–K  $\alpha$  radiation ( $\lambda = 0.154 \text{ nm}$ ), with a dwell time of  $2^\circ \text{ min}^{-1}$  and steps of  $0.02^\circ$ .

**2.1.4.5. Zeta potential.** Apparent zeta potential ( $\zeta$ ) of the suspensions were measured at  $25^\circ \text{C}$  by electrophoretic mobility through ZetaSizer (Nano Series ZS ZEN3600, Malvern, UK), using cuvettes DTS1070 (Malvern, UK). Samples were diluted to 0.01 wt % in ultrapure water prior to analysis.

#### 2.1.5. Polysaccharides isolation

AMP (Sigma-Aldrich) was dispersed in dimethyl sulfoxide and water (95:5) for 24 h, under magnetic stirring, at  $50 \text{ g L}^{-1}$ , after that the polysaccharide was precipitate in absolute ethanol. Purified AMP was filtered, and oven dried at  $30^\circ \text{C}$  in vacuum. Xyloglucan (XG) was obtained from commercial Tamarind seeds powder (DSP Gokyo Food & Chemicals). XG was dispersed in water at  $40 \text{ g L}^{-1}$  for 24 h, preserved with 200 ppm sodium azide ( $\text{NaN}_3$ ). After the polysaccharide was precipitated in 2 vol of absolute ethanol and dried in the same way as AMP. Molar mass of AMP and XG was  $4 \times 10^6$  and  $8 \times 10^4 \text{ g mol}^{-1}$ , respectively, as previously determined by Hazt et al. (2020).

#### 2.1.6. Emulsions preparation

Emulsions were prepared from stock dispersion of 10 wt % AMP and 2 wt % XG, preserved with 200 ppm of sodium azide. Following weighing, polysaccharides were mixed by vortex for 60 s. After that ultrapure water is added until the concentration of 1.02 wt % AMP and 1.30 wt % XG is reached, again the mixture is emulsified by vortex agitation for 60 s. CNPs were evaluated in concentrations ranging from 0.05 to 0.50 wt %. Macroscopic phase separation behavior was monitored for 168 h at  $21\text{--}24^\circ \text{C}$ .

### 2.1.7. Confocal laser scanning microscopy analysis of emulsions

For confocal laser scanning microscopy (CLMS) analysis of emulsions, AMP was labelled with fluorescein isothiocyanate (FITC) according to the methodology established by de Belder and Granath (1973). Emulsion was prepared with AMP containing 10 wt% of a FITC labelled AMP. CNPs were labelled using 5 ppm Nile blue dye, stirred overnight before use. Samples were placed in a glass bottom cell culture dish (Greiner Bio-one) and observed with water immersion objectives of 40x and 60x. Images were obtained by A1R MP Nikon CLMS with 561 nm (green) and 663 nm (red) excitation wavelengths.

### 2.1.8. Emulsions tilt test

To qualitatively evaluate emulsion stability, samples were tilted at 45° or 180° on a support. Emulsions flow was evaluated after 5 min of tilting samples containing CNPs after 168 h emulsification.

## 3. Results and discussion

### 3.1. Cellulose nanocrystals isolation and characterization

Sulfuric acid is recognized for isolating rod-like cellulose nanocrystals. In the case of MCC as starting material, the best conditions for reaction were established by Bondeson et al. (2006) using sulfuric acid at 63.5 wt% and obtaining 30 wt% yield after 2 h reaction. In our study for CNP-SH samples the yield was of 35 wt %. On the other hand, phosphoric acid is able to disrupt the intra and intermolecular hydrogen bonds in cellulose (Jia et al., 2013; Zhang et al., 2009). Once dissolved, cellulose can be precipitated (regenerated) in an antisolvent such as water (Hao et al., 2015). This procedure can alter the particle morphology and also their crystalline structure changing the cellulose allomorph type I to type II. Other methodologies, such mercerization, also can be applied with similar results.

Morphology discrepancy between sulfuric acid hydrolyzed MCC (CNP-SH), partial and quasi-totally desulfated CNP (CNP-D2, CNP-S1, respectively) and phosphoric acid dissolved and regenerated MCC (CNP-PH) can be clearly observed by the AFM images (Fig. 1).

CNP obtained from sulfuric acid hydrolysis (Fig. 1-A) exhibited a rod-like morphology as expected with a length of  $232 \pm 51$  nm, this value agreed with that reported by Bondeson et al. (2006) from 200 to 400 nm. Another feature of sulfuric acid hydrolysis was the introduction of anionic sulfate esters groups through surface CNP hydroxyls groups. This leads to CNPs particles repulsing each other when dispersed in water, promoting colloidal stability (Dufresne, 2013). Removing the surface sulfate groups from CNPs their stability was compromised and particles may aggregate more easily. It can be observed in CNP-D2 (Fig. 1-B) although their size remains at  $236 \pm 45$  nm it can be seen aggregated particles. When nearly all sulfate groups were removed (quasi-totally), like in CNP-S1 (Fig. 1-C), aggregation was more evident, and particles lies in  $268 \pm 52$  nm. Jiang et al. (2010) reports a very similar behavior for fully desulfated CNPs aggregating in endwise manner resembling elongated particles.

An alternative route to produce cellulose nanoparticles with distinct morphology was from nanoprecipitation. After adding phosphoric acid solubilized cellulose in water, and after regeneration spherical particles, CNP-PH, with  $60 \pm 11$  nm were obtained (Fig. 1-D). Size values reported in this present paper differ from Hao et al. (2015), which reports spherical CNPs with diameters ranging from 500 to 600 nm and aggregates to 1–2  $\mu\text{m}$ . Even if conditions for CNPs isolating were similar experimental factors such solvent/antisolvent ratio can result in the particle size range (Chin, Jimmy, & Pang, 2018).

Surface groups (sulfate or phosphate) can be quantified by conductometric titration. Since the excess hydronium ions were removed during dialysis step, CNPs were eluted on an ion exchange column to assure protonation of all sulfate or phosphate groups. Fig. S1 shows the titration plots of sulfated and phosphated CNPs suspensions. Initially, with base addition, hydrogens linked to functional surface groups were

consumed indicated by a linear decrease in conductivity. After neutralization the conductivity increases linearly due to the remaining hydroxyl ions of base in solution.

According to Eq. (1) was possible to quantify CNP surface groups, the value for CNP-SH was  $203 \pm 3$  mmol  $\text{kg}^{-1}$ . After two desulfation cycles using hydrochloric acid the result decreases to  $107 \pm 1$  mmol  $\text{kg}^{-1}$  representing  $\sim 53\%$  of initial sulfate content. This was very consistent with has been obtained in literature (Jiang et al., 2010). Solvolysis desulfation was able to remove  $\sim 90\%$ , promoting a quasi-totally desulfation from the initial value, resulting in  $20 \pm 1$  mmol  $\text{kg}^{-1}$ .

It is also possible to quantify the phosphate groups by the same titration technique the obtained result for CNP-PH was  $160 \pm 4$  mmol  $\text{kg}^{-1}$ . This value was higher than those reported in the literature, which ranges from 8 to 45 mmol  $\text{kg}^{-1}$  (Vanderfleet, Osorio, & Cranston, 2018). However, it is important to emphasize in this case that starting material is different resulting in rod-like phosphate CNPs as opposed to the spherical ones reported in present work.

Surface groups in this manuscript were directly associated with colloidal stability, which can be quantified by zeta potential of suspensions. CNP-SH, with higher sulfate group content presents a  $-31 \pm 2$  mV potential while values of  $-25 \pm 4$  mV and  $-13 \pm 5$  mV were measured for CNP-D2 and CNP-S1, respectively. Reduction in zeta potential values was coincident with removal of surface groups and this also explains aggregation observed in AFM images (Fig. 1-A, B, C).

CNP-PH particles has  $-5 \pm 2$  mV of zeta potential, a relatively low values, compared to CNP-SH, CNP-D2 and CNP-S1, since it has a considerable amount of phosphate groups on its surface as evidenced by conductometric titration. An important point to highlight is that for all samples Smoluchowski's model was used for apparent zeta potential analysis, overestimating the potential measured due to particle anisotropy. So, it is not straightforward to compare CNP-PH, an apparently isotropic particle, with CNP-PH, CNP-D2 and CNP-S1 samples based on apparent zeta potentials.

The reason for a lower colloidal stability of CNP-PH, comparing the phosphate quantification ( $160$  mmol  $\text{kg}^{-1}$ ) and apparent zeta potential, was related to particles surface area, and that phosphate groups, accessed during titration, are not at the particle interface. Also, in case of CNP-SH surface area was approximated  $4600$  nm<sup>2</sup> considering a rodlike approximation, and by other hand, phosphated CNP has an area of  $\sim 11,000$  nm<sup>2</sup>, considering the spheroidal shape. Although CNP-PH presents  $160$  mmol  $\text{kg}^{-1}$ , when compared to sulfates CNPs the charge density per area is much lower.

Particles that have low colloidal stability tend to agglomerate over time. Techniques such as probe-type ultrasound improve the dispersion by breaking clusters (Asadi et al., 2019). This procedure can be on-line coupled with apparent hydrodynamic diameter ( $D_{\text{app}}$ ) measurement by DLS (Fig. S2). Two situations can be observed regarding sonication: (i) when it was used during entire experiment or (ii) when it was used for a limited time before measurement. In first case, no aggregates were formed, and in this condition  $D_{\text{app}}$  of CNP-PH is  $77 \pm 2$  nm, slightly higher than values observed via AFM. This is because DLS measurements are performed with particles in suspension, unlike AFM. In second case a limited energy is supplied to suspension and ensures that it becomes dispersed into individual particles. After ceasing energy, it is possible to note that  $\sim 100$  s later the  $D_{\text{app}}$  considerably increases indicating cluster formation ( $>200$  nm). The fast aggregation produces large particles with time (above micrometers) which have interesting properties that will be discussed later. In summary, DLS results showed that CNC-PH particles tend to aggregate over time.

Besides changing shape, it is possible to change cellulose allomorph due to mercerization or regeneration process. Crystalline domains of cellulose can be organized at molecular level in different configurations. Native cellulose generally presents the type I polymorph, characterized by a triclinic ( $I_{\alpha}$ ) or monoclinic ( $I_{\beta}$ ) unit cell, both in a parallel chain. If chains are organized in antiparallel configuration, it is possible to get another polymorph type II which is more stable than type I (Jin et al.,

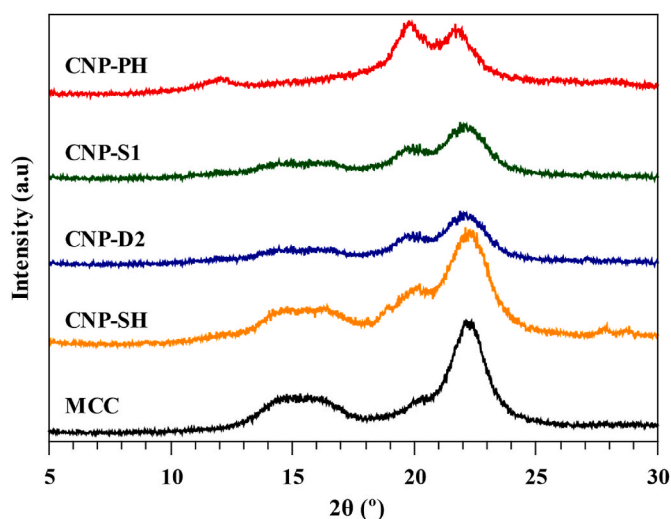


Fig. 2. XRD diffractograms for sulfated (CNP-SH, D2 and S1) and phosphated (CNP-PH) cellulose samples, both obtained from the same source (MCC).

2016). One method to determine polymorphism is through XRD technique. Diffractograms of MCC and the sulfated and phosphate nanosized cellulose was presented in Fig. 2.

Diffractometer peaks reveal Miller's indices related to crystalline structure. For type I cellulose, there were three characteristics peaks at  $2\theta = 23.0^\circ$ ,  $16.0^\circ$  and  $14.5^\circ$  related to the (200), (110) and (010) indices, respectively. For type II cellulose at  $2\theta = 22.0^\circ$ ,  $20.0^\circ$  and  $12.0^\circ$  there were peaks related to (020), (110) and (010) indices, respectively (French, 2014). MCC, CNP-D2 and CNP-S1 exhibits three characteristics peaks of type I cellulose. This showed that during hydrolysis with sulfuric acid and desulfation there was no conversion to other polymorphs. On the other hand, the reaction with phosphoric acid was able to convert the polymorph to type II cellulose, and in this case, there was cellulose regeneration.

Table 1 summarizes the main characteristics of isolated CNPs. Hydrolysis using sulfuric acid allowed isolation of CNPs with same morphological features and allomorph, whose surface sulfate content can be modulated by acid-catalyzed desulfation or solvolysis. Using phosphoric acid, with same raw material for CNPs isolation, it is possible to obtain spherical particles by dissolving and precipitating cellulose, also changing its allomorph. This ensure an arsenal of different particles for stabilizing AMP/XG emulsions as will be discussed hereafter.

Table 1

Summary of the main properties of nanocellulose particles obtained from MCC.

Sample	Treatment	Morphology	Allomorph	Dimensions (nm)	Apparent zeta potential (mV)	Sulfate groups (mmol kg <sup>-1</sup> )	Phosphate groups (mmol kg <sup>-1</sup> )
CNP-SH	H <sub>2</sub> SO <sub>4</sub> hydrolysis	Rod-like	I	232 ± 51	-31 ± 2	203 ± 3	-
CNP-D2	Acid Desulfation			236 ± 45	-25 ± 4	107 ± 1	-
CNP-S1	Solvolytic Desulfation			258 ± 62	-13 ± 5	20 ± 1	-
CNP-PH	H <sub>3</sub> PO <sub>4</sub> hydrolysis	Spherical	II	60 ± 11	-5 ± 2	-	160 ± 4

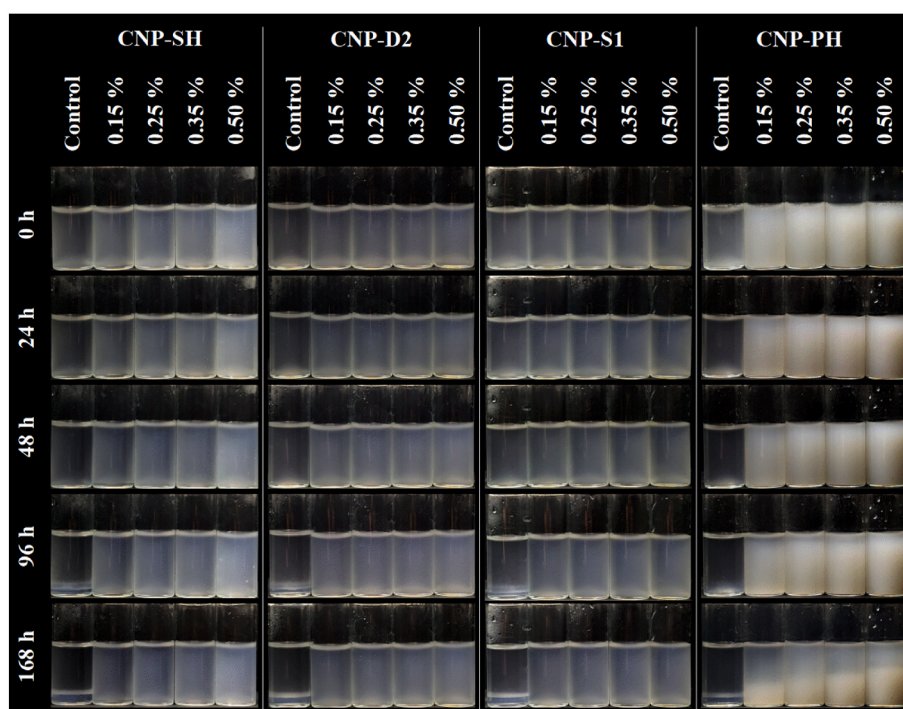
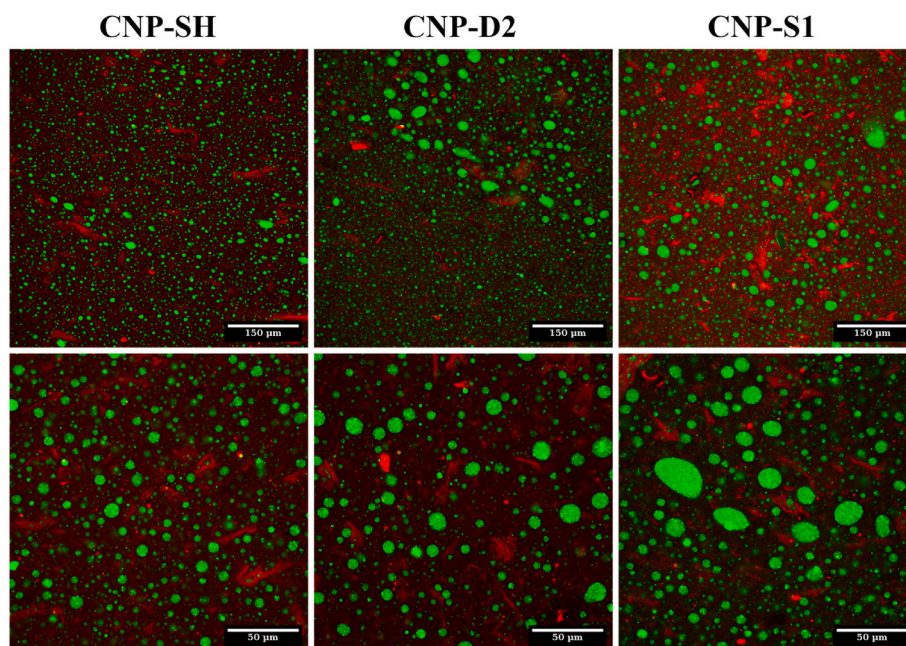
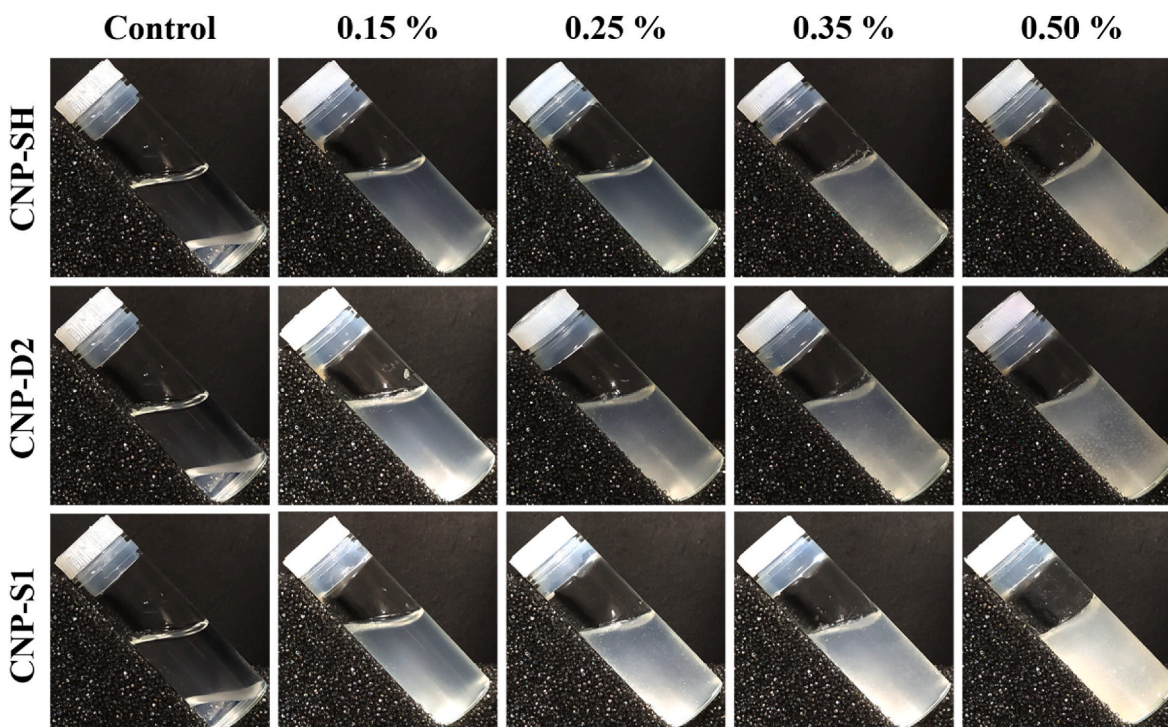


Fig. 3. Macroscopic behavior evaluation of AMP (1.02 wt %) in XG (1.30 wt %) in absence of particles (control) and at different concentrations of sulfated CNPs (SH, D2 and S1) and phosphates (PH).



**Fig. 4.** Confocal laser scanning microscopy for AMP (1.02%) in XG (1.30%) emulsions with 0.5% sulfated CNPs after 1 h emulsification. AMP presents the green color and CNPs red.



**Fig. 5.** AMP (1.02 wt %) in XG (1.30 wt %) emulsions observed in the presence of sulfated CNPs and absence of particles (control). The tube tilted at 45° qualitatively shows that higher CNP concentration form gels, stabilizing the emulsions.

### 3.2. Water-in-water emulsions

Concentrations of 1.02 wt% AMP and 1.30 wt% XG were chosen to evaluate behavior of CNPs in emulsions stabilization. At these biopolymers' concentration emulsions XG is continuous phase, as described in phase diagram (Hazi et al., 2020). Four CNPs concentrations were tested ranging from 0.15 to 0.50 wt%.

Fig. 3 shows the w/w emulsions macroscopic results. In particles

absence (control), in all cases, w/w emulsions start phase separation from 48 h becoming even more evident after 96 h and total at 168 h. Sulfated CNPs, regardless their sulfate content (CNP-SH, CNP-D2 and CNP-S1) stabilize emulsions. Macroscopically, no phase separation could be observed at small CNPs concentrations. In contrast, phosphated CNPs (CNP-PH) begin phase separation from 48 h extending up to 168 h. However, unlike control, it can be observed that there is still an emulsified fraction corresponding to particle concentration, even increasing

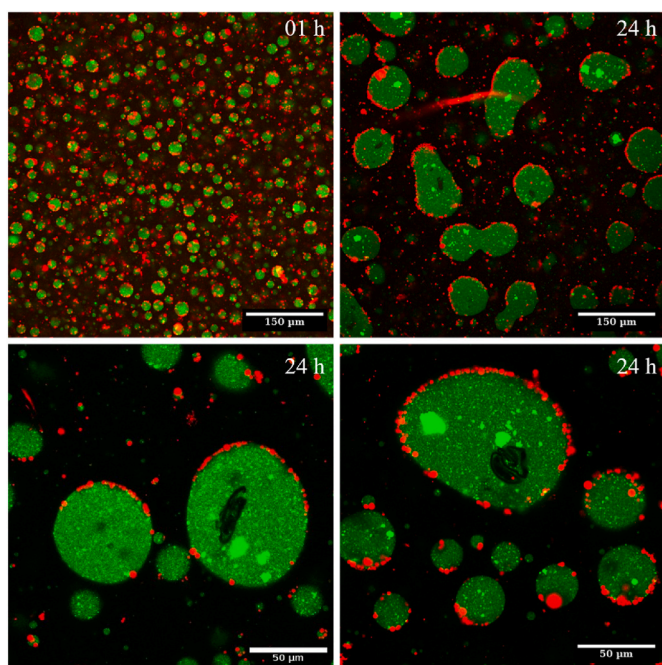


**Fig. 6.** Confocal laser scanning microscopy for AMP (1.02 wt%) in XG (1.30 wt %) emulsions with 0.50 wt % phosphate CNPs in red color at interface of AMP, in green.

CNP-PH concentrations up to 1.50 wt% (Fig. S3).

For a more detailed investigation, microscopic evaluations were performed using confocal microscopy. FITC-labelled AMP displays green color as a dispersed phase in emulsion and the CNPs particles in red, marked by Nile Blue at images. In Fig. 4 it can clearly be seen that there is no evidence of CNPs particles at AMP interface even at highest concentration (0.50 wt%), independent of surface content of the samples. That is, Pickering mechanism stabilization was not evidenced in this case.

Reason for emulsion stabilization facing sulfated CNPs can be explained from interactions between these polysaccharides, specially XG-CNPs. In plant cell wall, cellulose plays the role of a reinforcement material that holds together the hemicellulose network. Cellulose-XG affinity is mainly due to the high hydroxyl content forming hydrogen bonds and also hydrophobic interactions (Morris, Hanna, & Miles, 2004). It is also known that the interactions between XG and CNP in water can form hydrogels. Talantikite, Gourlay, Le Gall, and Cathala (2019) explored the effect of XG molar mass on these materials' formation, noting that XG of higher molar mass form viscous liquids and gels with particular CNPs concentrations. That is, higher XG molar mass and higher CNP concentration favor the gel formation.

Fig. 5 shows tubes containing sulfated CNPs emulsions tilted at 45°. This angle allows a qualitative observation of emulsions' flow after 168 h. Without CNPs it is possible to observe that emulsion flowed tilting the tube. CNPs at 0.50 wt% concentration, independent of sulfate content, promoted a notable resistance to flow, indicating a greater solid-like behavior, forming strong gels (Fig. S4). Considering that XG is the continuous phase of the emulsion, the increase of its solid-like behavior of the continuous phase with sulfated CNPs impacts on the AMP droplets coalescence, promoting emulsion stability by a cold gelation process, and consequently prevents phase separation, justifying the emulsion stability.

On the other hand, phosphates CNPs exhibit a different behavior. Fig. 6 shows emulsions at 1 h and 24 h after emulsification. At initial time it is possible to observe smaller AMP droplets (Fig. 6, green) in presence of phosphated CNPs particles at interface (Fig. 6, red). After 24 h, larger AMP droplets are evident and some particles are still resident at

interface.

This demonstrates that CNP-PH migrate at interface as in Pickering emulsions, in a opposed way observed for sulfated CNPs. However, the interface coating was not complete, even at high CNPs concentration, and coalescence is not completely prevented (Fig. 3).

It is also possible to notice that phosphated CNPs that are at AMP interface presents a considerable large diameter than the isolated particles (lies in 1–3 µm), this can be justified due a low colloidal stability of these particles, evidenced by a low potential zeta value, inducing the aggregation observed by DLS (Fig. 3) as a time function, suggesting that CNP-PH particles form large flocks in solution prior to interfacial adsorption. As the desorption energy increased with the square of the particle size, it evident that particle association bring positive effects on emulsion stability.

Besides morphology, crystalline structure is one of the major differences between the evaluated particles. Sulfate CNPs presents type I allomorph while phosphated type II. In addition, cellulose has an amphiphilic character presenting a hydrophilic region due to its hydroxyls in the side chain and a hydrophobic region due to C–H axial bonds in chain. Regenerated cellulose (type II) exposes more the (010) crystalline plane which is related to the equatorial hydroxyls, as result of higher density of exposed hydroxyls this allomorph becomes more hydrophilic (Yamane et al., 2006). So, XG chains interact non-covalently with the most hydrophobic region of CNPs (Park & Cosgrove, 2015; Zhao, Crespi, Kubicki, Cosgrove, & Zhong, 2014), and this justifies the preferential interaction of sulfated CNPs not allowing them to migrate at emulsion interface.

#### 4. Conclusion

The hypothesis that the sulfate ester content of CNPs affect the preferential interaction with XG and thus could migrate to the XG/AMP water in water emulsion interface was tested from three distinct sulfate contents with different CNPs concentrations. Macroscopically the emulsions were shown stable for up to 168 h. However, microscopically no crystals, regardless of sulfate content, was evident at system interface. In other words, hypothesis was not confirmed. Additional tests prove that in the presence of sulfated CNPs the continuous phase (XG) viscosity increases, impeding the AMP droplets coalescence, thus stabilizing the emulsions. On the other hand, with the same starting material through a simple solubilization with phosphoric acid follow by a water regeneration it is possible to obtain another cellulose particles and allomorph. Due to its more hydrophilic nature, the interaction with XG is disfavored allowing particles to migrate to system interface forming Pickering emulsions, at least in the initial hours. Thus, the hydrophilicity of phosphated CNPs was more determinant for interfacial adsorption particles compared to the sulfate content of sulfated CNPs.

#### Author statement

**Cassiano Pires:** Conceptualization, Methodology, Formal Analysis, Investigation, Writing – Original Draft.

**Bernardo Mauad Régnier:** Methodology, Formal Analysis, Investigation.

**Maria Jackeline Rodrigues dos Santos:** Formal Analysis.

**Rilton Alves de Freitas:** Conceptualization, Methodology, Funding acquisition, Supervision, Writing – Review & Editing.

#### Declaration of competing interest

The authors declare that they have no known competing financial interests or personal relationships that could have appeared to influence the work reported in this paper.

## Data availability

Data will be made available on request.

## Acknowledgements

The authors greatly acknowledge the Center of Advanced Fluorescence Technologies (CTAF-UFPR) for CLSM analysis, and Paraná Federal University (UFPR) for the technical and scientific assistance provided. Cassiano Pires, Bernardo M. Régner and Maria Jackeline R. dos Santos are grateful for doctoral and scientific initiation program received from CAPES and CNPq, respectively. Rilton A. de Freitas is Research Member of the National Research Council of Brazil (CNPq) (no 305768/2021-2). This study was financed in part by the Coordenação de Aperfeiçoamento de Pessoal de Nível Superior – Brasil (CAPES) – Finance Code 001, CAPESPRINT 41/2017 (no 88887.311748/2018-00) and CNPq (430451/2018-0).

## Appendix A. Supplementary data

Supplementary data to this article can be found online at <https://doi.org/10.1016/j.foodhyd.2023.108700>.

## References

- Asadi, A., Pourfattah, F., Miklós Szilágyi, I., Afrand, M., Żyła, G., Seon Ahn, H., et al. (2019). Effect of sonication characteristics on stability, thermophysical properties, and heat transfer of nanofluids: A comprehensive review. *Ultrasonics Sonochemistry*, 58, Article 104701. <https://doi.org/10.1016/j.ultsonch.2019.104701>
- Balakrishnan, G., Nicolai, T., Benyahia, L., & Durand, D. (2012). Particles trapped at the droplet interface in water-in-water emulsions. *Langmuir*, 28(14), 5921–5926. <https://doi.org/10.1021/la204825f>
- Beck, S., Méthot, M., & Bouchard, J. (2015). General procedure for determining cellulose nanocrystal sulfate half-ester content by conductometric titration. *Cellulose*, 22(1), 101–116. <https://doi.org/10.1007/s10570-014-0513-y>
- Beldengrün, Y., Dallaris, V., Jaén, C., Protat, R., Miras, J., Calvo, M., et al. (2020). Formation and stabilization of multiple water-in-water-in-water (W/W/W) emulsions. *Food Hydrocolloids*, 102, Article 105588. <https://doi.org/10.1016/j.foodhyd.2019.105588>
- de Belder, A. N., & Granath, K. (1973). Preparation and properties of fluorescein-labelled dextrans. *Carbohydrate Research*, 30(2), 375–378. [https://doi.org/10.1016/S0008-6215\(00\)81824-8](https://doi.org/10.1016/S0008-6215(00)81824-8)
- Ben Ayed, E., Cochereau, R., Dechancé, C., Capron, I., Nicolai, T., & Benyahia, L. (2018). Water-in-water emulsion gels stabilized by cellulose nanocrystals. *Langmuir*, 34(23), 6887–6893. <https://doi.org/10.1021/acs.langmuir.8b01239>
- Bondeson, D., Mathew, A., & Oksman, K. (2006). Optimization of the isolation of nanocrystals from microcrystalline cellulose by acid hydrolysis. *Cellulose*, 13(2), 171–180. <https://doi.org/10.1007/s10570-006-9061-4>
- Chin, S. F., Jimmy, F. B., & Pang, S. C. (2018). Size controlled fabrication of cellulose nanoparticles for drug delivery applications. *Journal of Drug Delivery Science and Technology*, 43, 262–266. <https://doi.org/10.1016/j.jddst.2017.10.021>
- Dufresne, A. (2013). Nanocellulose: A new ageless bionanomaterial. *Materials Today*, 16(6), 220–227. <https://doi.org/10.1016/j.mattod.2013.06.004>
- Esquena, J. (2016). Water-in-water (W/W) emulsions. *Current Opinion in Colloid & Interface Science*, 25, 109–119. <https://doi.org/10.1016/j.cocis.2016.09.010>
- Foster, E. J., Moon, R. J., Agarwal, U. P., Bortner, M. J., Bras, J., Camarero-Espinosa, S., et al. (2018). Current characterization methods for cellulose nanomaterials. *Chemical Society Reviews*, 47(8), 2609–2679. <https://doi.org/10.1039/C6CS00895J>
- de Freitas, R. A., Nicolai, T., Chassenieux, C., & Benyahia, L. (2016). Stabilization of water-in-water emulsions by polysaccharide-coated protein particles. *Langmuir*, 32(5), 1227–1232. <https://doi.org/10.1021/acs.langmuir.5b03761>
- French, A. D. (2014). Idealized powder diffraction patterns for cellulose polymorphs. *Cellulose*, 21(2), 885–896. <https://doi.org/10.1007/s10570-013-0030-4>
- Frith, W. J. (2010). Mixed biopolymer aqueous solutions – phase behaviour and rheology. *Advances in Colloid and Interface Science*, 161(1–2), 48–60. <https://doi.org/10.1016/j.cis.2009.08.001>
- Gonzalez-Jordan, A., Nicolai, T., & Benyahia, L. (2016). Influence of the protein particle morphology and partitioning on the behavior of particle-stabilized water-in-water emulsions. *Langmuir*, 32(28), 7189–7197. <https://doi.org/10.1021/acs.langmuir.6b01993>
- Habibi, Y., Lucia, L. A., & Rojas, O. J. (2010). Cellulose nanocrystals: Chemistry, self-assembly, and applications. *Chemical Reviews*, 110(6), 3479–3500. <https://doi.org/10.1021/cr900339w>
- Hao, X., Shen, W., Chen, Z., Zhu, J., Feng, L., Wu, Z., et al. (2015). Self-assembled nanostructured cellulose prepared by a dissolution and regeneration process using phosphoric acid as a solvent. *Carbohydrate Polymers*, 123, 297–304. <https://doi.org/10.1016/j.carbpol.2015.01.055>
- Hazt, B., Bassani, H. P., Elias-Machado, J. P., Aldinucci Buzzo, J. L., Silveira, J. L. M., & de Freitas, R. A. (2020). Effect of pH and protein particle shape on the stability of amylopectin-xyloglucan water-in-water emulsions. *Food Hydrocolloids*, 104, Article 105769. <https://doi.org/10.1016/j.foodhyd.2020.105769>
- Jia, X., Chen, Y., Shi, C., Ye, Y., Wang, P., Zeng, X., et al. (2013). Preparation and characterization of cellulose regenerated from phosphoric acid. *Journal of Agricultural and Food Chemistry*, 61(50), 12405–12414. <https://doi.org/10.1021/jf4042358>
- Jiang, F., Esker, A. R., & Roman, M. (2010). Acid-catalyzed and solvolytic desulfation of H<sub>2</sub>SO<sub>4</sub>-hydrolyzed cellulose nanocrystals. *Langmuir*, 26(23), 17919–17925. <https://doi.org/10.1021/la1028405>
- Jin, E., Guo, J., Yang, F., Zhu, Y., Song, J., Jin, Y., et al. (2016). On the polymorphic and morphological changes of cellulose nanocrystals (CNC-I) upon mercerization and conversion to CNC-II. *Carbohydrate Polymers*, 143, 327–335. <https://doi.org/10.1016/j.carbpol.2016.01.048>
- Lei, C., Xie, Y., Wu, Y., Li, Y., Li, B., Pei, Y., et al. (2022). Properties and stability of water-in-water emulsions stabilized by microfibrillated bacterial cellulose. *Food Hydrocolloids*, 130, Article 107698. <https://doi.org/10.1016/j.foodhyd.2022.107698>
- Morris, S., Hanna, S., & Miles, M. J. (2004). The self-assembly of plant cell wall components by single-molecule force spectroscopy and Monte Carlo modelling. *Nanotechnology*, 15(9), 1296–1301. <https://doi.org/10.1088/0957-4484/15/9/031>
- Nguyen, B. T., Wang, W., Saunders, B. R., Benyahia, L., & Nicolai, T. (2015). PH-responsive water-in-water pickering emulsions. *Langmuir*, 31(12), 3605–3611. <https://doi.org/10.1021/la5049024>
- Nicolai, T., & Murray, B. (2017). Particle stabilized water in water emulsions. *Food Hydrocolloids*, 68, 157–163. <https://doi.org/10.1016/j.foodhyd.2016.08.036>
- Norton, I. T., & Frith, W. J. (2001). Microstructure design in mixed biopolymer composites. *Food Hydrocolloids*, 15(4–6), 543–553. [https://doi.org/10.1016/S0268-005X\(01\)00062-5](https://doi.org/10.1016/S0268-005X(01)00062-5)
- Park, Y. B., & Cosgrove, D. J. (2015). Xyloglucan and its interactions with other components of the growing cell wall. *Plant and Cell Physiology*, 56(2), 180–194. <https://doi.org/10.1093/pcp/pcu204>
- Peddiredy, K. R., Nicolai, T., Benyahia, L., & Capron, I. (2016). Stabilization of water-in-water emulsions by nanorods. *ACS Macro Letters*, 5(3), 283–286. <https://doi.org/10.1021/acsmacrolett.5b00953>
- Pirich, C. L., de Freitas, R. A., Woehl, M. A., Picheth, G. F., Petri, D. F. S., & Sierakowski, M. R. (2015). Bacterial cellulose nanocrystals: Impact of the sulfate content on the interaction with xyloglucan. *Cellulose*, 22(3), 1773–1787. <https://doi.org/10.1007/s10570-015-0626-y>
- Talantikite, M., Gourlay, A., Le Gall, S., & Cathala, B. (2019). Influence of xyloglucan molar mass on rheological properties of cellulose nanocrystal/xyloglucan hydrogels. *Journal of Renewable Materials*, 7(12), 1381–1390. <https://doi.org/10.32604/jrm.2019.07838>
- Trache, D., Tarchoun, A. F., Derradji, M., Hamidon, T. S., Masruchin, N., Brosse, N., et al. (2020). Nanocellulose: From fundamentals to advanced applications. *Frontiers of Chemistry*, 8, 392. <https://doi.org/10.3389/fchem.2020.00392>
- Vanderfleet, O. M., Osorio, D. A., & Cranston, E. D. (2018). Optimization of cellulose nanocrystal length and surface charge density through phosphoric acid hydrolysis. *Philosophical Transactions of the Royal Society A: Mathematical, Physical & Engineering Sciences*, 376(2112), Article 20170041. <https://doi.org/10.1098/rsta.2017.0041>
- Vis, M., Opdam, J., van 't Oor, I. S. J., Soligno, G., van Roij, R., Tromp, R. H., et al. (2015). Water-in-Water emulsions stabilized by nanoplates. *ACS Macro Letters*, 4(9), 965–968. <https://doi.org/10.1021/acsmacrolett.5b00480>
- Yamane, C., Aoyagi, T., Ago, M., Sato, K., Okajima, K., & Takahashi, T. (2006). Two different surface properties of regenerated cellulose due to structural anisotropy. *Polymer Journal*, 38(8), 819–826. <https://doi.org/10.1295/polymj.PJ2005187>
- Zhang, J., Zhang, J., Lin, L., Chen, T., Zhang, J., Liu, S., et al. (2009). Dissolution of microcrystalline cellulose in phosphoric acid—molecular changes and kinetics. *Molecules*, 14(12), 5027–5041. <https://doi.org/10.3390/molecules14125027>
- Zhao, Z., Crespi, V. H., Kubicki, J. D., Cosgrove, D. J., & Zhong, L. (2014). Molecular dynamics simulation study of xyloglucan adsorption on cellulose surfaces: Effects of surface hydrophobicity and side-chain variation. *Cellulose*, 21(2), 1025–1039. <https://doi.org/10.1007/s10570-013-0041-1>
- Zhou, C., Xie, Y., Li, Y., Li, B., Zhang, Y., & Liu, S. (2023). Water-in-water emulsion stabilized by cellulose nanocrystals and their high enrichment effect on probiotic bacteria. *Journal of Colloid and Interface Science*, 633, 254–264. <https://doi.org/10.1016/j.jcis.2022.11.051>